

Article

Gas–Liquid Two-Phase Upward Flow through a Vertical Pipe: Influence of Pressure Drop on the Measurement of Fluid Flow Rate

Tarek A. Ganat ^{1,*}  and Meftah Hrairi ² 

¹ Department of Petroleum Engineering, Universiti Teknologi PETRONAS, Seri Iskandar, Perak 32610, Malaysia

² Department of Mechanical Engineering, International Islamic University Malaysia, P.O. Box 10, Kuala Lumpur 50728, Malaysia; meftah@iiu.edu.my

* Correspondence: tarekarbi.ganat@utp.edu.my; Tel.: +60-53687111

Received: 23 June 2018; Accepted: 31 August 2018; Published: 27 October 2018



Abstract: The accurate estimation of pressure drop during multiphase fluid flow in vertical pipes has been widely recognized as a critical problem in oil wells completion design. The flow of fluids through the vertical tubing strings causes great losses of energy through friction, where the value of this loss depends on fluid flow viscosity and the size of the conduit. A number of friction factor correlations, which have acceptably accurate results in large diameter pipes, are significantly in error when applied to smaller diameter pipes. Normally, the pressure loss occurs due to friction between the fluid flow and the pipe walls. The estimation of the pressure gradients during the multiphase flow of fluids is very complex due to the variation of many fluid parameters along the vertical pipe. Other complications relate to the numerous flow regimes and the variabilities of the fluid interfaces involved. Accordingly, knowledge about pressure drops and friction factors is required to determine the fluid flow rate of the oil wells. This paper describes the influences of the pressure drop on the measurement of the fluid flow by estimating the friction factor using different empirical friction correlations. Field experimental work was performed at the well site to predict the fluid flow rate of 48 electrical submersible pump (ESP) oil wells, using the newly developed mathematical model. Using Darcy and Colebrook friction factor correlations, the results show high average relative errors, exceeding $\pm 18.0\%$, in predicted liquid flow rate (oil and water). In gas rate, more than 77% of the data exceeded $\pm 10.0\%$ relative error to the predicted gas rate. For the Blasius correlation, the results showed the predicted liquid flow rate was in agreement with measured values, where the average relative error was less than $\pm 18.0\%$, and for the gas rate, 68% of the data showed more than $\pm 10\%$ relative error.

Keywords: pressure loss; pressure drop; friction factor; multiphase flow; flow rate; flow regime

1. Introduction

In the oil and gas industry, multiphase flow in vertical pipes often occurs. The flow of fluids through the vertical pipe string causes a loss of energy through friction losses, where the value of this loss depends on the fluid flow viscosity and the size of the conduit. Often, the friction loss is an important part of the oil well completion design [1]. The pressure drop occurs as a result of the changes in potential and kinetic energy of the fluid due to the friction on the pipe walls [2]. Generally, the total pressure drop in the vertical conduit is basically related to four main components: frictional, hydrostatic, acceleration, and pressure drop. Among these four components, calculation of the pressure drop is the most complex component and has received extensive attention by researchers [3,4]. Many researchers have attempted to determine the two-phase frictional pressure drop over the whole range

of flow patterns through a vertical pipe. A substantial number of experiments have been carried out to determine fluid flow friction losses in both Newtonian [1,2,5–11] and non-Newtonian systems [5,12]. A large number of experimental works was made in short tubes. Consequently, a lot of engineering problems come up when efforts are made to extend these experimental results to real oil field conditions where a longer pipe is used. In those experiments, the data shows only a limited number of variables, and as a result, imprecisions are introduced when the friction correlations are applied outside the limitations of the experimental data. As a consequence of the limited amount of data available for these experiments, the effects of some significant variables were ignored in the early studies [13–17]. The accuracy of the pressure drop prediction in flowing wells has a significant influence on the fluid flow measurement. There are many particular solutions, but they are valid only for some specific conditions. This is due to the complexity of two-phase flow analysis. In some conditions, the gas travels at a much higher velocity than the liquid. Accordingly, the flowing density of the gas–liquid mixture is higher than the corresponding density. Moreover, the liquid’s velocity inside the pipe wall can be different over a short distance and can cause a variable friction loss. The difference in velocity and flow regime of the two phases strongly affect pressure drop computations [13], meaning that slippage is a consequence of the difference between the combined velocities of the two phases, which is caused by the physical properties of the fluids involved. For single-phase flow, the frictional pressure losses do not normally increase with a decrease in the tubing size or an increase in well production flow rate. This refers to the existence of a gas phase, which tends to slip by the liquid phase without essentially contributing to its lift. Many researchers have tried to show a relationship between the slippage losses and the friction losses [15–18]. A method for the estimation of gas–liquid flow rates in the vertical pipe has been proposed [19]. The method was used to calibrate a differential pressure sensor to predict the flow rates of both phases in air–water flow. The estimations were in good agreement with real flow rate measurements. A study by Daev and Kairakbaev [20] proposed a new model of the liquid flow through pipes that incorporated flow straighteners. The prediction of the flow rate of liquid was studied and the parameters affecting the process of measuring the flow rate of liquid were considered. An experimental study of the two-phase flow regime and frictional pressure drop inside the pipe was done by Cai et al. [21]. The flow patterns were defined and recorded by a high-speed camera. A new empirical correlation was proposed based on the experimental results to predict the liquid multiplier factor of the test channel. A two-phase flow measurement applying a resistive void fraction meter combined to a venturi, or orifice plate, was suggested by Oliveira et al. [22]. This method was applied to determine the fluid mass flow rates using an air–water experimental apparatus. The results showed that the flow path has no important effect on the meters in relation to the frictional pressure drop in the experimental process range. The outcomes of the experimental work displayed a mean slip ratio of less than 1.1, when slug and bubbly flow patterns were lower than 70%.

This research work aims to evaluate the influence of a pressure drop on the measurement of the fluid flow rate in ESP oil wells. A new mathematical model was developed to determine the fluid flow rate of the oil wells through the prediction of multiphase flow parameter variations inside a vertical pipe based on local temperature and pressure changes with depth and applying multiphase flow physics equations and empirical correlations. The objective of this study was to obtain data from well tests conducted in a long vertical pipe and utilize this data to evaluate the effects of slippage and friction factor, in different flow regimes, on the calculation accuracies of the fluid flow rate of the oil wells. The approach measured the liquid hold-up along the conduit and used different friction correlations such as Blasius, Darcy, and Colebrook friction factor correlations to compare the predicted fluid flow rate with the measured fluid flow rate for each oil well. Generally, the results show that any errors in pressure drop calculation will generate inaccuracies in the prediction of fluid flow rate.

2. Experimental Arrangements and Measurement Procedure

The experiments conducted in the present study were carried out for two-phase flow through a vertical pipe of 48 oil wells using ESP pumps. A schematic of the experimental system is shown in Figure 1. The flow measurement starts at the surface wellhead, and then down to the bubble point pressure location depth in the well. Wellhead flowing pressure was measured at normal production conditions before and after the wing valve shut-in, leaving the ESP pump running, to measure the build-up of pressure at the wellhead. The total shut-in time period of the wellhead valve was then recorded. The first free gas bubbles started liberating from the bubble point location depth inside the tubing string. This occurred in the production flowing well before and after the wellhead wing valve shut-in, and the changes of flow patterns inside the pipe were reallocated once again, due to variations of temperature and pressure along the conduit. As a consequence, the liberated gas was dissolved in the oil phase, and the location depth of the bubble point pressure relocated to another position after the wellhead wing valve shut-in. The column of liquid that replaced the liberated gas column space, during the shut-in time period, was the difference between the first and second bubble point location depths. Figure 2 shows the bubble point location depths before and after the wellhead wing valve shut-in. A conceptual basis of physics for prediction of fluid flow rate in the conduit was employed along with multiphase empirical correlations to compute the variations of fluid flow parameters inside the tubing.

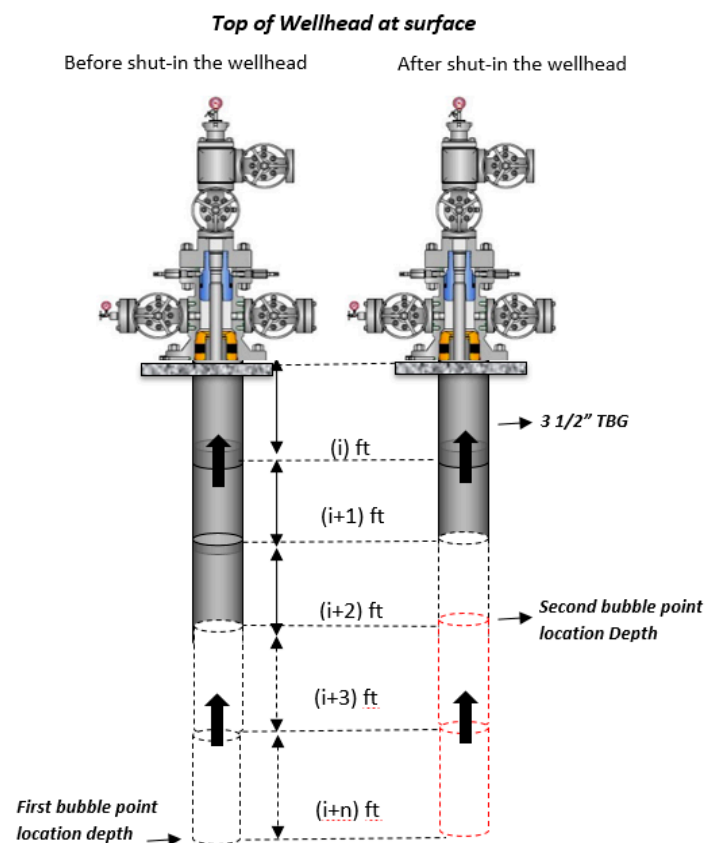


Figure 1. Schematic of the flow measurement stages in a vertical pipe before and after the well head wing valve shut-in.

Several assumptions were made to conduct the calculations such as: assumed one-dimensional flow in the conduit, assumed uniform cross-sectional area of the pipe, the phase's properties varied with depth, the frictional factor varied along the conduit, and the effect of the liquid compressibility was neglected.

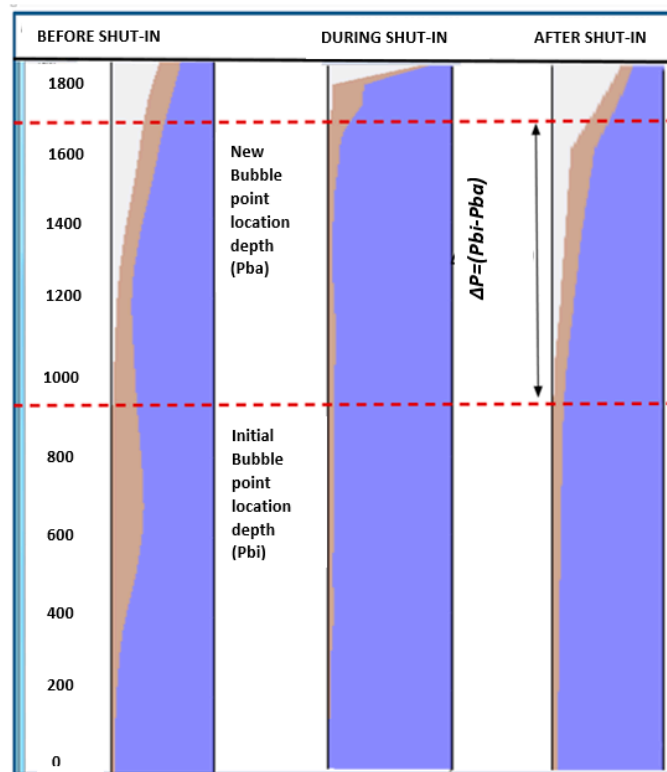


Figure 2. Bubble point location depths before and after closing the well head wing valve.

2.1. Required Input Data

The input data required were the well parameters data and physical properties data of the fluid, as seen in Table 1. To carry out this study, 48 ESP oil wells were selected where the wells were producing from four different reservoirs using same production pipe diameter. Also, these reservoirs had almost the same reservoir fluid properties: the bubble point pressure ranged from 924 psi to 1124 psi, the American Petroleum Institute (API) oil gravity ranged from 36 to 37 @ 60 °F, the oil viscosity ranged from 0.784 cP to 1.0119 cP, and the reservoir temperature ranged from 157 °F to 186 °F. Furthermore, Figure 3 classifies the input data required.

Table 1. Well and physical properties of the fluid.

Well Name	WHPb (PSIA)	WHPa (PSIA)	WHT (F)	GOR (SCE/STB)	WC (%)	Total Shut-in Time (min)
A33	140	200	98	360.92	93	1.55
A125	100	200	95	360.92	91.62	0.83
A64	180	250	107	360.92	81.52	1.06
A29	250	270	107	360.92	84.88	0.80
A23	210	260	127.7	360.92	82.11	0.24
A135	210	250	100	360.92	59.88	0.56
A126	250	300	98	360.92	66.91	0.20
A12	175	270	107	360.92	82.9	0.84
A108	260	300	97	360.92	81.31	0.28
5J5	150	300	95	360.92	4	3.36
5J2	100	170	101	360.92	52	1.39
5J4	250	300	101.6	360.92	58.95	0.27
5J7	250	300	98	360.92	30	0.47
E89	150	190	140	300	79	0.27
E210	80	120	110	300	83	0.33

Table 1. Cont.

Well Name	WHPb	WHPa	WHT	GOR	WC	Total Shut-in Time
	(PSIA)	(PSIA)	(F)	(SCE/STB)	(%)	(min)
E211	80	120	129	300	74	0.96
E286	70	100	146	300	90	0.25
E192	80	110	146	300	83	0.24
E327	80	110	115.5	300	77	0.35
E325	70	110	124.6	300	83	0.44
E197	90	110	146.1	300	82	0.11
E208	95	110	146.8	300	81	0.07
E226	80	110	138.4	300	91	0.25
E284	80	120	124.5	300	76	0.33
E258	65	90	142	300	86	0.23
E326	60	100	113	300	82	0.48
E227	100	150	142	300	84	0.36
4E_3	130	300	146	300	87	1.18
B56	120	170	120	384	42	2.3
B70	160	230	120	384	29.9	2.9
B121	100	160	120	364	67.29	0.5
B119	100	160	120	364	76.18	1.1
B50	180	250	110	364	68.65	0.55
B88	100	160	110	364	63.59	2.1
B14	250	270	110	364	76.28	0.15
B151	180	230	110	364	55.78	0.66
B164	100	170	120	364	26.3	2.1
B51	240	310	120	364	59.05	0.44
Q89	100	150	120	364	0	3.7
Q21	80	150	120	364	79.22	2.1
Q53	80	150	120	364	71.41	2.3
Q14	75	130	120	364	74.83	1.4
Q100	80	130	110	364	78.27	0.55
Q12	80	150	110	364	80.33	0.58
Q85	100	150	110	364	18.18	2.5
Q82	100	150	110	364	75.3	0.5
Q78	80	150	120	364	37.27	2.5
Q76	80	150	120	364	80.5	1.3

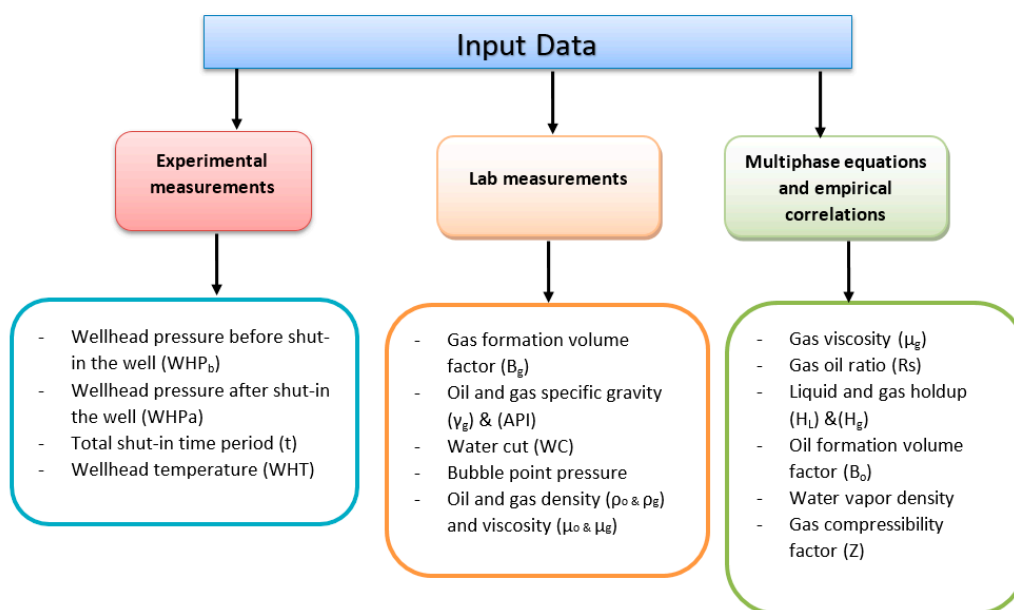


Figure 3. Input data required.

2.2. Computational Algorithm

Figure 4 shows the algorithm steps to evaluate the mathematical model. The algorithm classified all the main stages and sub-steps in the model. In this process, the calculations were performed to obtain the bubble point pressure location depth before and after the wellhead wing valve shut-in. The fluid flowing pressure gradient could be calculated anywhere inside the pipe. All the variables needed to be identified to correctly evaluate the physics interactions between all the fluid parameters using the suitable multi-physics equations and empirical correlations.

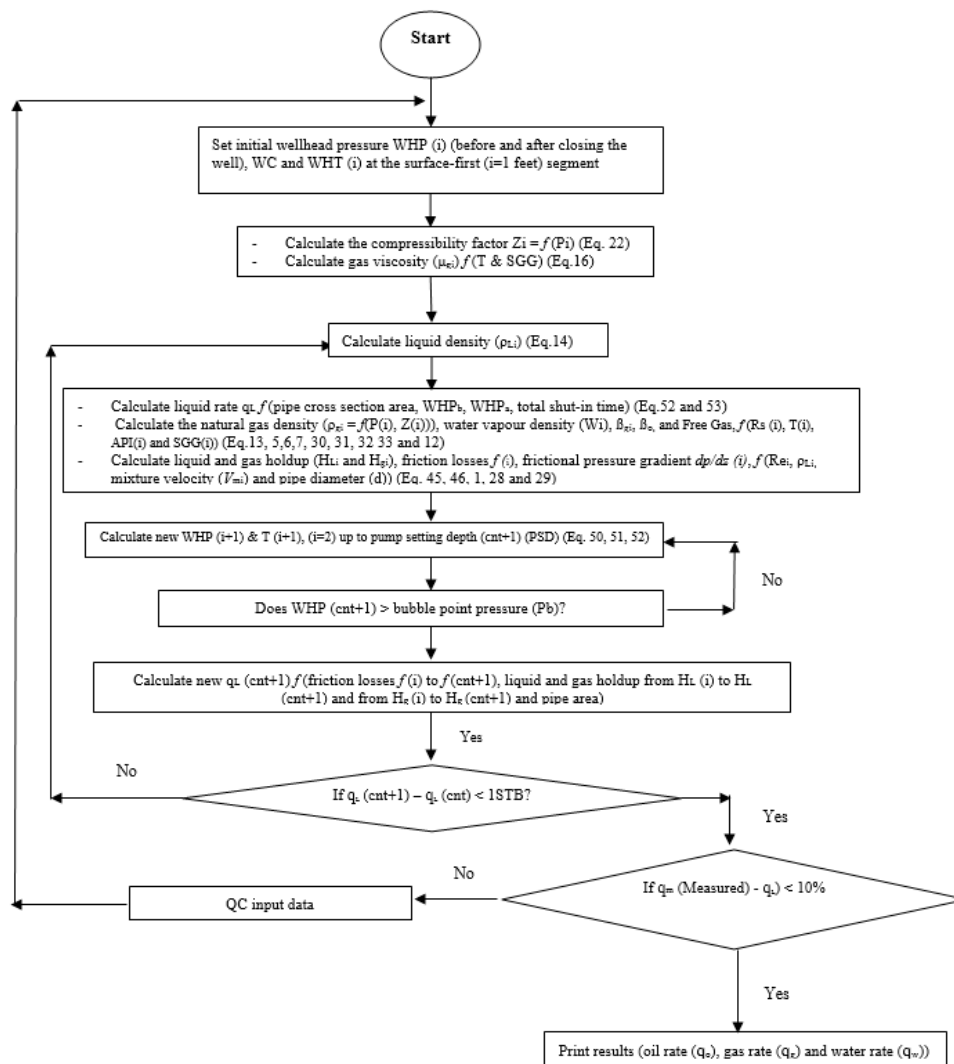


Figure 4. Flowchart of the new mathematical model algorithm.

The calculation starts at the surface wellhead and then down to the location depth of the bubble point pressure as a function of temperature and pressure variations with depth. To consider the fact that flow regimes vary depending on the in situ flow rates of gas/liquid, the model calculates, at each foot along the vertical pipe, the variations of supercritical velocities, viscosities, and densities for both phases (liquid and gas). The in situ flow rate can also be calculated by the mathematical model at any flow regime at any depth. As shown in Figures 5 and 6, the calculation iteration can stop at any depth (i, ..., i + n) using all the equations (from Equation (1) to Equation (56)), where there is a different flow regime along the vertical pipe.

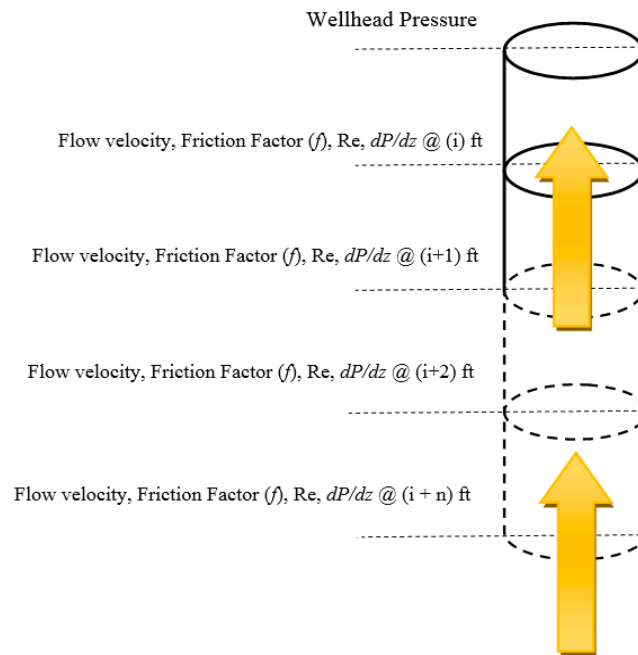


Figure 5. Stages of computational methodology.

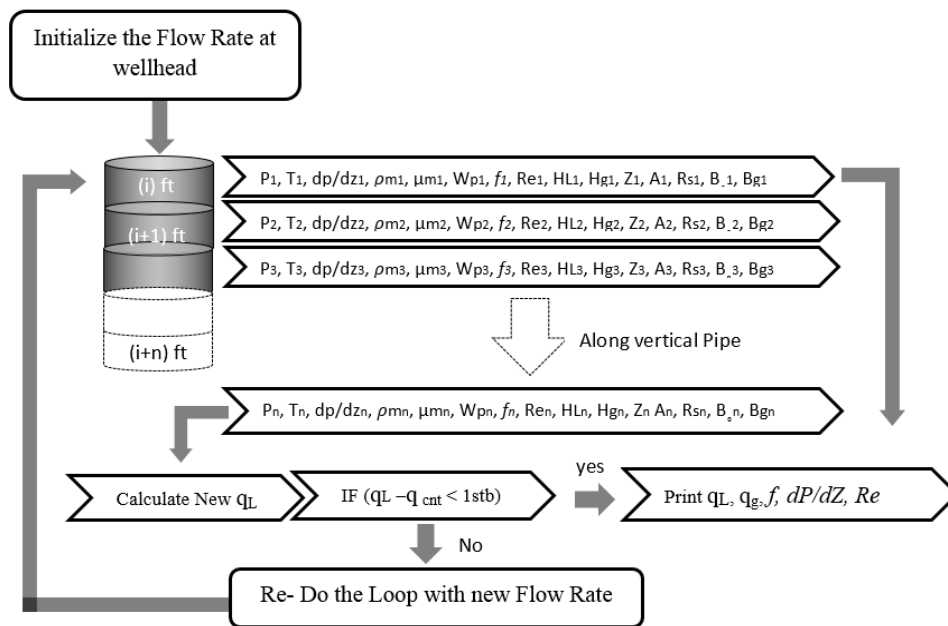


Figure 6. Flow diagram of new computational method procedure.

The following are the physics equations and the correlations applied to determine each independent variable at every single foot.

Total pressure losses expressed as

$$\Delta P_{Total} = \Delta P_{HH} + \Delta P_{Frictional} \tag{1}$$

Hydrostatic head is expressed as

$$\Delta P_{HH} = \frac{\rho_m g \Delta Z}{144 g_c} \tag{2}$$

Darcy–Weisbach equation [23] was used to calculate the frictional pressure loss

$$\Delta P = f \frac{L}{D} \frac{\rho V^2}{2} \quad (3)$$

Reynolds number is given by

$$Re = \frac{2.2 \times 10^{-2} m_t}{D \mu_L^{H_L} \mu_g^{(1-H_L)}} \quad (4)$$

Three different friction factor correlations were applied to evaluate the impact of the friction on the computation of the fluid flow rate. The first correlation is the Blasius empirical correlation for turbulent flow [24].

$$f = 0.316 (Re)^{-0.25} \quad (5)$$

The second friction correlation applied is Darcy correlation [23]

$$f = \frac{64}{Re} \quad (6)$$

The third friction factor correlation applied is from Colebrook [25]

$$\frac{1}{\sqrt{f}} = 2 \log_{10} \left(\frac{\varepsilon/D_h}{3.7} + \frac{2.51}{Re \sqrt{f}} \right) \quad (7)$$

for $Re < \approx 2300$ and $Re > \approx 4000$.

The gas density is expressed as

$$\rho_g = \frac{m_g}{V_R} = \frac{M_g P}{ZRT} \quad (8)$$

The density at wellbore condition, is given by

$$\rho_g = \frac{\rho_{gs}}{B_g} \quad (9)$$

The oil density is expressed as

$$\rho_o = \frac{62.428 \gamma_o + 0.014 \gamma_g R_s}{B_o} \quad (10)$$

where

$$\gamma_o = \rho_o / \rho_w \quad (11)$$

$$\gamma_g = \frac{\rho_g}{\rho_{air}} = \frac{\rho_g}{0.077} \quad (12)$$

$$\rho_g = 0.077 \gamma_g \quad (13)$$

Liquid density is given by

$$\rho_L = \rho_W WC + \rho_o (1 - WC) \quad (14)$$

Mixture density is expressed as

$$\rho_m = \rho_L H_L + \rho_g (1 - H_L) \quad (15)$$

The gas viscosity is determined by the following equation [26]:

$$\mu_g = K_1 \exp(X \rho^Y) \quad (16)$$

where

$$\rho = \frac{pM_g}{zRT} = 0.0015 \frac{pM_g}{zT} \quad (17)$$

$$K_1 = \frac{(0.001 + 2 \times 10^{-6} M_g) T^{1.5}}{(209 + 19M_g + T)} \quad (18)$$

$$X = 3.5 + \frac{986}{T} + 0.01M_g \quad (19)$$

$$Y = 2.4 - 0.2X \quad (20)$$

Mixture viscosity is given by

$$\mu_m = \mu_L^{H_L} + \mu_g^{(1-H_L)} \quad (21)$$

Beggs and Brill equation [27] was applied to estimate the gas compressibility factor (Z)

$$Z = A + \frac{(1-A)}{e^B} + CPr^D \quad (22)$$

Using Standing and Katz equations [28] to obtain the pseudo critical temperature and pressure of the gas mixture

$$Pr = 688.634 - 21.983\gamma_g - 13.886\gamma_g^2 \quad (23)$$

$$Tr = 158.01 + 342.12\gamma_g - 16.04\gamma_g^2 \quad (24)$$

and

$$A = 1.39(Tr - 0.92)^{0.5} - 0.36Tr - 0.101 \quad (25)$$

$$B = (0.62 - 0.23Tr)Pr + \left(\frac{0.066}{Tr - 0.86} - 0.037 \right) Pr^2 + \frac{0.32}{10^{9(Tr-1)}} Pr^2 \quad (26)$$

$$C = 0.132 - 0.32 \log(Tr) \quad (27)$$

$$D = 10^{(0.302 - 0.49Tr + 0.182Tr^2)} \quad (28)$$

Superficial gas velocity is expressed as

$$V_{sg} = \frac{4q_g B_g}{\pi D^2} \quad (29)$$

Superficial liquid velocity is expressed as

$$V_{sL} = \frac{4q_L}{\pi D^2} \quad (30)$$

The water vapor density using the Sloan correlation [29] is expressed as

$$W = \exp\left(c_1 + \frac{c_2}{T} + c_3 \ln(p) + \frac{c_4}{T^2} + \frac{c_5 \ln(P)}{T} + c_6 (\ln(P))^2\right) \quad (31)$$

where the values of constants c_1 to c_6 are shown in Table 2.

Table 2. Constants c_1 to c_6 .

Constants	Value
c_1	28.911
c_2	-9668.146
c_3	-1.663
c_4	-130,823.5
c_5	205.323
c_6	0.0385

The gas formation volume factor is expressed as

$$B_g = \frac{P_{sc} Z T}{T_{sc} P} = 0.028 \frac{Z T}{P} \quad (32)$$

Using the Vasquez and Beggs equation [30] to obtain the oil formation volume factor

$$B_{ob} = 1 + C_1 R_{sb} + C_2 (T - 60) \left(\frac{\gamma_{API}}{\gamma_g} \right) + C_3 R_{sb} (T - 60) \left(\frac{\gamma_{API}}{\gamma_g} \right) \quad (33)$$

and oil gas ratio

$$R_{sb} = \frac{\gamma_g P b C_2}{C_1} 10^{\left(\frac{C_3 \gamma_{API}}{T + 459.67} \right)} \quad (34)$$

where the coefficients C_1 , C_2 and C_3 are given by

Coefficient	$^{\circ}\text{API} \leq 30$	$^{\circ}\text{API} \geq 30$
C_1	27.64	56.060
C_2	1.0937	1.187
C_3	11.172	10.393

To make sure that the obtained liquid and gas hold-up is accurate, some popular correlations, used by the industry and are included in almost every commercial software package, were considered to predict the liquid and gas hold-up inside each well. The correlations considered in this study are the ones developed by Hagedorn and Brown [31], Duns and Ros [32], Orkiszewski [33], and Aziz et al. [34]. The statistical results for the various prediction methods when applied to all 25 well tests are shown in Figure 7 and Table 3. These results indicate that the Hagedorn and Brown correlation seems to predict liquid and gas hold-up better than the other correlations selected in this study. However, the overall results show minor differences between the different correlations. This is because each correlation was developed based on certain assumption and for a particular range of data.

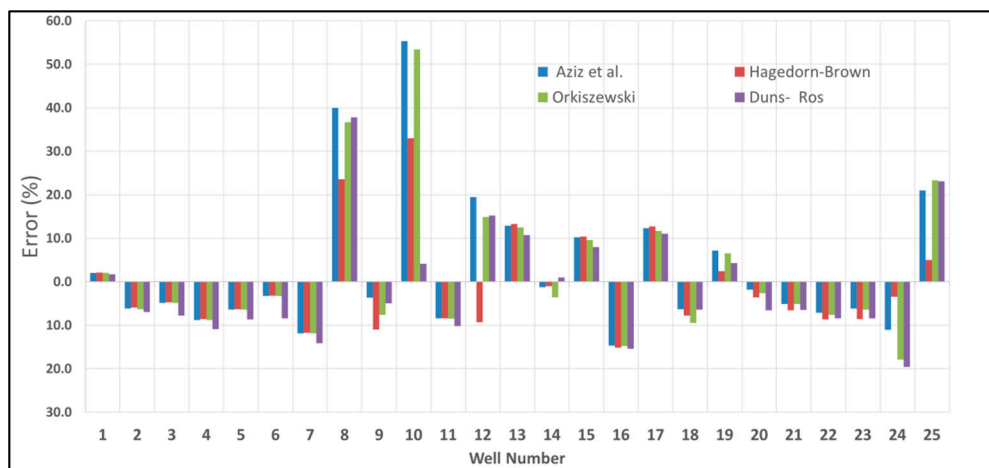


Figure 7. Hold-up prediction accuracy using some popular correlations.

Table 3. Statistical results for the various prediction correlations.

Prediction Method	Average Error	Standard Deviation
	(%)	(%)
Duns and Ros	−1.06	13.06
Hagedorn and Brown	−0.86	11.57
Orkiszewski	1.8	16.52
Aziz et al.	2.9	16.66

Using the Hagedorn-Brown empirical correlation [31] to obtain liquid and gas hold-up (H_L and H_g)

$$N_{Lv} = 1.938v_{sL} \frac{\sqrt[4]{\rho}}{\sigma} \quad (35)$$

$$N_{gv} = 1.938v_{sg} \sqrt[4]{\frac{\rho_L}{\sigma}} \quad (36)$$

$$N_d = 120.872D \frac{\sqrt{\rho_L}}{\sigma} \quad (37)$$

$$N_L = 0.157\mu_L \sqrt[4]{\frac{1}{\rho_L\sigma^3}} \quad (38)$$

$$Y = -2.699 + 0.158X_1 - 0.551X_1^2 + 0.548X_1^3 - 0.122X_1^4 \quad (39)$$

where

$$X_1 = \log(N_L + 3) \quad (40)$$

$$CN_L = 10^Y \quad (41)$$

$$\frac{H_L}{\psi} = -0.103 + 0.618(\log X_2 + 6) - 0.633(\log X_2 + 6)^2 + 0.296(\log X_2 + 6)^3 - 0.04(\log X_2 + 6)^4 \quad (42)$$

where

$$X_2 = \frac{N_{VL}P^{0.1}CN_L}{N_{Vg}^{0.575}Pa^{0.1}N_D} \quad (43)$$

$$\psi = 0.912 - 4.822X_3 + 1232.25X_3^2 - 22253.6X_3^3 + 116174.3X_3^4 \quad (44)$$

where

$$X_3 = \frac{N_{Vg}N_L^{0.38}}{N_D^{2.14}} \quad (45)$$

The liquid hold-up is

$$H_L = \psi \left(\frac{H_L}{\psi} \right) \quad (46)$$

and

$$H_g = (1 - H_L) \quad (47)$$

The liquid flow rate is expressed as

$$q_L = \frac{\Delta H \cdot A}{t} \quad (48)$$

the cross section of the conduit is given by

$$A = \frac{\pi r^2}{4} \quad (49)$$

$$\Delta H = H_2 - H_1 \quad (50)$$

as

$$\Delta P = \Delta H \cdot \rho_L \quad (51)$$

then

$$\Delta H = \frac{\Delta P}{\rho_L} \quad (52)$$

and

$$\Delta P = WHP_a - WHP_b \quad (53)$$

then

$$q_L = \Delta P \frac{A}{\rho_L} t \quad (54)$$

The flow rates for gas, oil, and water are expressed as

$$q_o = q_L(1 - WC) \quad (55)$$

$$q_g = q_o R_s \quad (56)$$

$$q_w = q_o WC \quad (57)$$

3. Results and Discussion

The experiments were run on 48 ESP oil wells from four different reservoirs. For each friction factor correlation, the measured oil flow rate values for each oil well were compared against the predicted flow rate values. It should be noted that as the points near the dotted straight line drawn at 45° (i.e., $y = x$) in the graph, the more accurate the prediction was. The results show that the pressure drop value was the significant parameter that had the main influence on the fluid flow rate computation. Indeed, any errors in pressure drop values would lead to high uncertainty errors of fluid flow rate prediction. For this reason, the properties of independent variables needed to be considered. Likewise, the interactions between each phase needed to be taken into account along with mixture properties and in situ volume fractions of oil and gas inside the conduit. Each multiphase flow correlation found the friction factor differently. Typically, each friction correlation made its own assumptions and modifications to make them useable to multiphase conditions. The prediction of frictional pressure drop in two-phase flow was usually complicated due to pressure and temperature variations along the flow path. When estimating the friction factor, there were a number of methods for calculating the Reynolds number depending on how much of the two-phase flow mixture was defined. Therefore, the oil and water were considered as a single liquid phase while the gas was considered as a separate phase.

By using the Blasius friction factor correlation, the differences between the predicted flow rate and the measured flow rate were very small. R-squared (R^2) explained exactly how the data points were fitted close to the regression line ($y = x$). Figures 8–10 displayed the regression model for oil, water, and gas flow rate measurements. It can be seen that the plots show that most data points lie on or close to the unit slope line (e.g., best fit line), indicating that the predicted and actual values were in excellent agreement and illustrated an accurate flow rate prediction for oil, water, and gas with good correlating coefficients of 0.994, 0.993, and 0.966, respectively. This means that 99.4%, 99.3%, and 96.6% of the variance in the oil, water, and gas data, respectively, was explained by the line and 0.6%, 0.7%, and 3.4% of the variance was due to unexplained effects. The figures show that the predicted wells flow rates fell within the accepted uncertainty when compared with the measured flow rates.

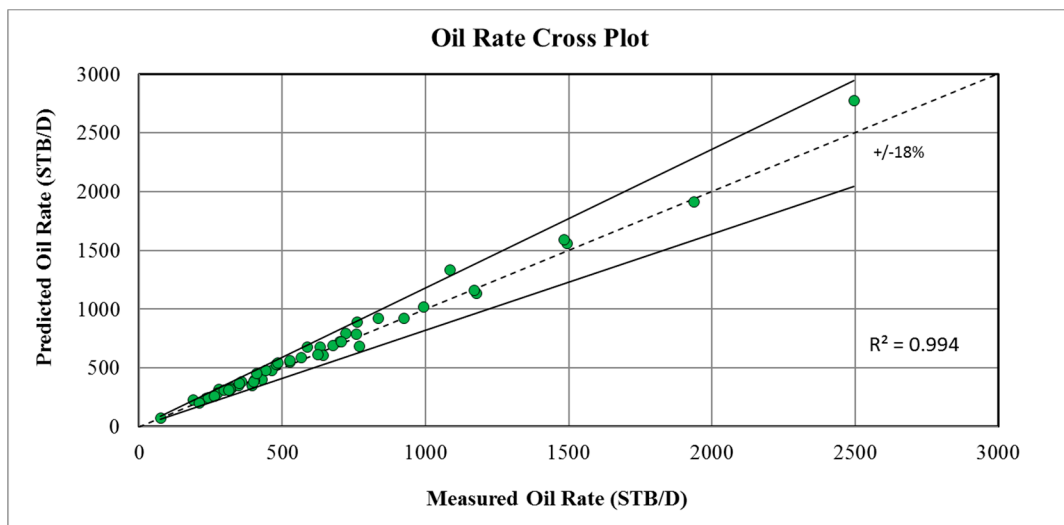


Figure 8. Predicted vs measured oil rate using the Blasius correlation.

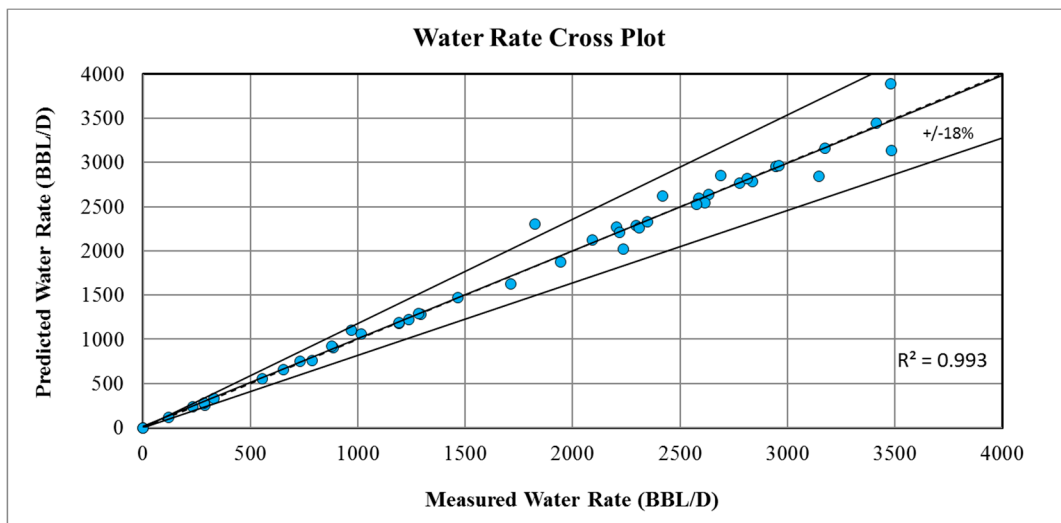


Figure 9. Predicted vs measured water rate using the Blasius correlation.

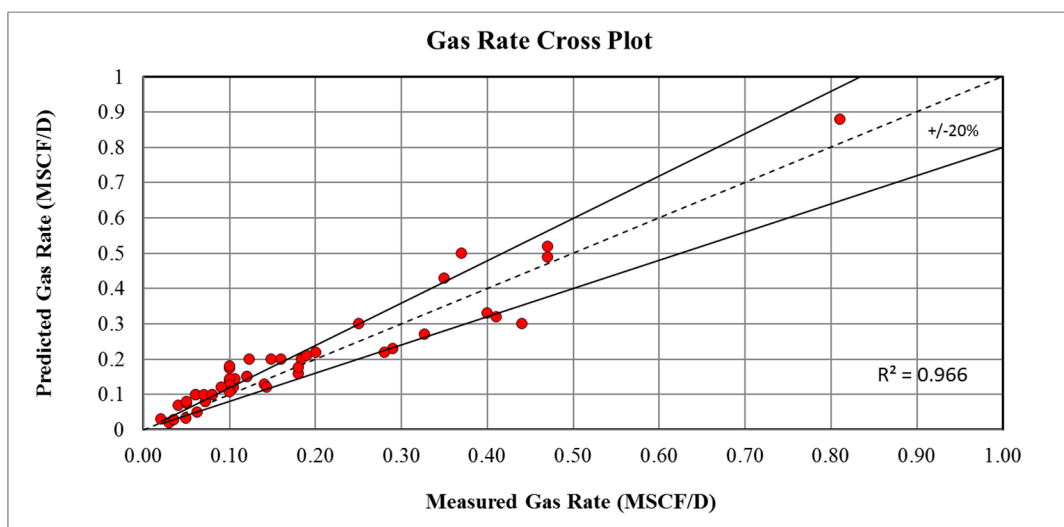


Figure 10. Predicted vs measured gas rate using the Blasius correlation.

By using the Darcy friction factor correlation, the differences between the predicted fluid flow rates with the measured flow rates were larger than those of the Blasius correlation. Figures 11–13 displayed the regression model for oil, water, and gas flow rate measurements. From these figures, one can easily recognize that the data plotted is under-estimated for oil and water flow rates and scattered around the best fit line for gas flow rates. This discrepancy was more evident for high flow rates where the correlation coefficients for oil, water, and gas flow rates accounted for 90.6%, 86.6%, and 78.7% of the variance, respectively. The figures show that the predicted well flow rates did not fall within the accepted uncertainty when compared with the measured flow rates.

By using the Colebrook friction factor correlation, the differences between the predicted fluid flow rates with the measured flow rates were slightly better than the Darcy correlation performance, but still less than the Blasius correlation performance. Figures 14–16 displays the data fitting for oil, water, and gas flow rate measurements. Similar to the performance of the Darcy correlation, one can easily recognize that the data plotted is under-estimated for oil and water flow rates and scattered around the best fit line for gas flow rates. This discrepancy was more evident for high flow rates where the correlation coefficients for oil, water, and gas flow rates accounted for 93.0%, 87.1%, and 80.8% of the variance, respectively. The figures showed that the predicted wells flow rates did not fall within the accepted uncertainty when compared with the measured flow rates.

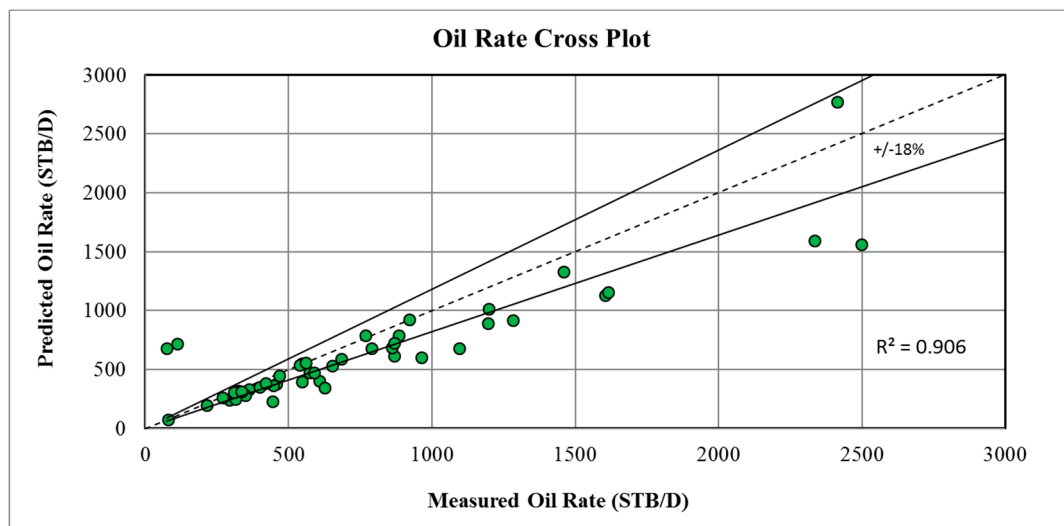


Figure 11. Predicted vs measured oil rate using the Darcy correlation.

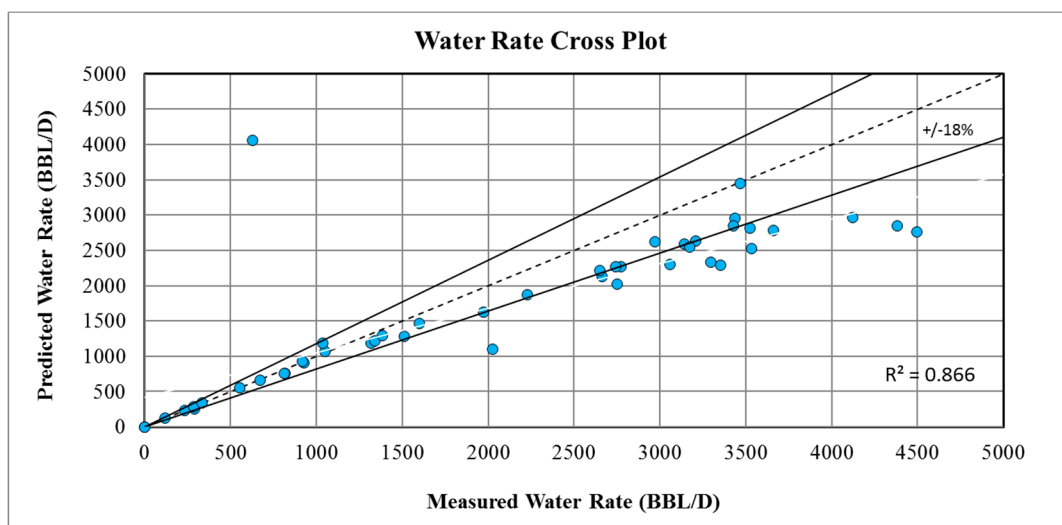


Figure 12. Predicted vs measured water rate using the Darcy correlation.

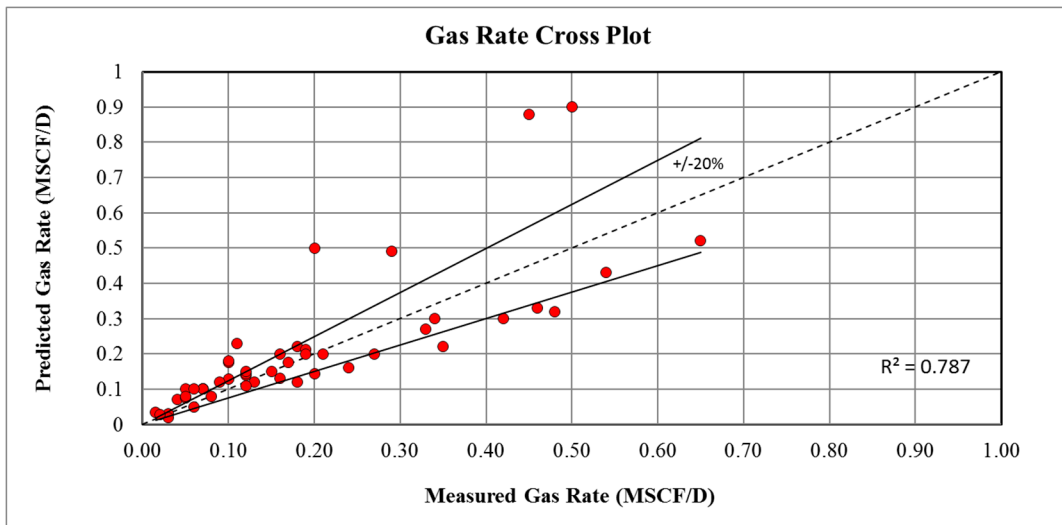


Figure 13. Predicted vs measured gas rate using the Darcy correlation.

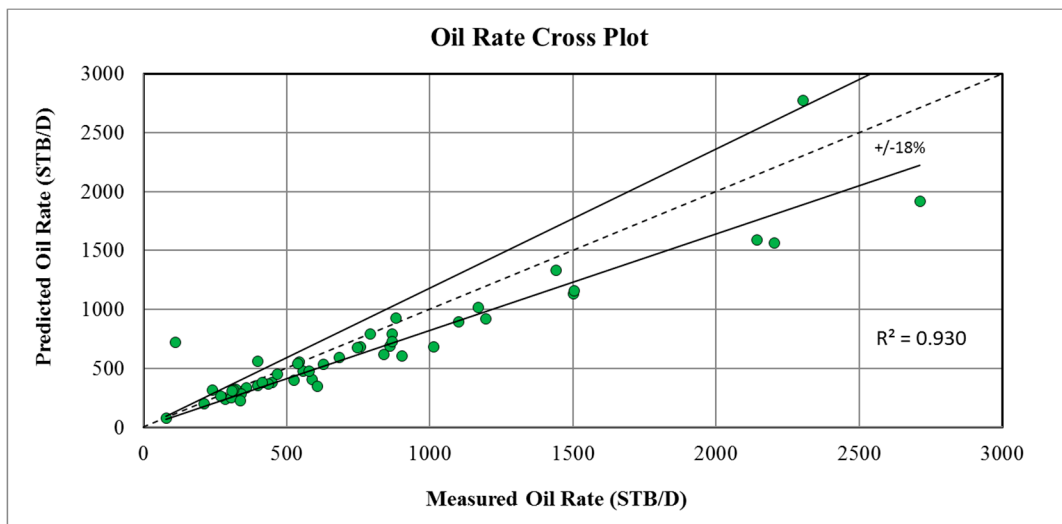


Figure 14. Predicted vs measured oil rate using the Colebrook correlation.

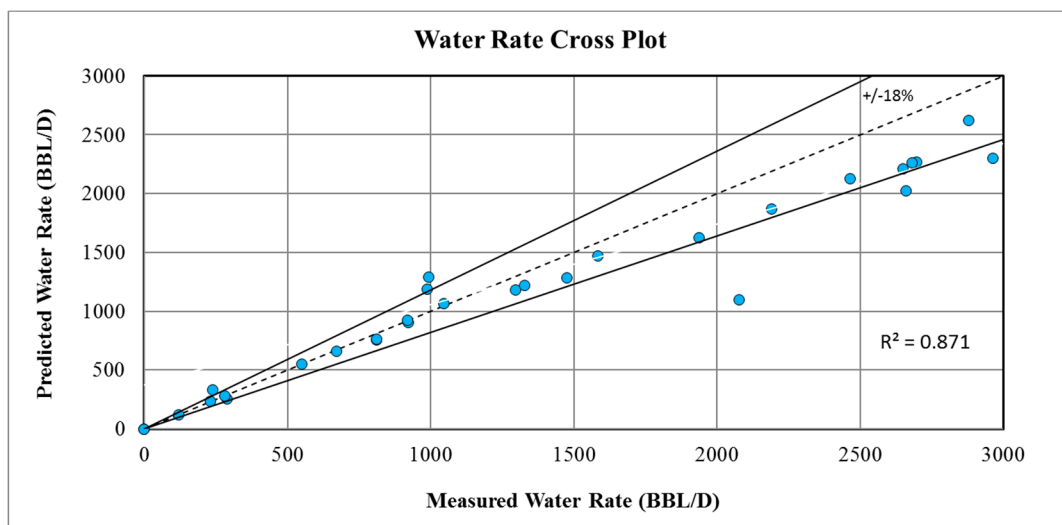


Figure 15. Predicted vs measured water rate using the Colebrook correlation.

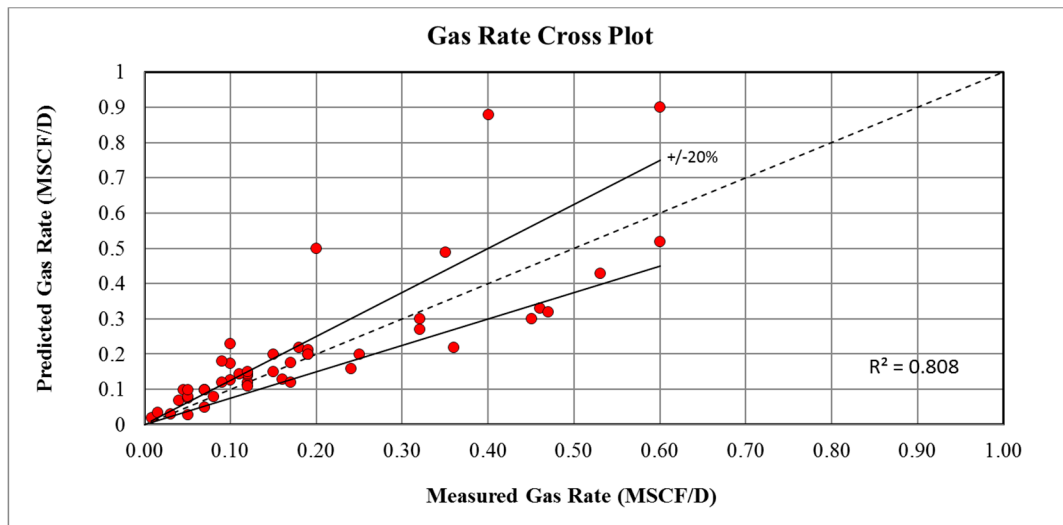


Figure 16. Predicted vs measured gas rate using the Colebrook correlation.

In general, the validation results of the predicted fluid flow rates were satisfactory when using the Blasius correlation rather than the Darcy or Colebrook correlations, where 96% and 98% of the predicted fluid flow rates were in good agreement with the real measured oil and water flow rate, respectively. Furthermore, the relative errors were less than $\pm 18\%$, which were still within the reasonable uncertainty, as shown in Figures 17 and 18. For the predicted and measured gas rates, 68% of the wells showed about $\pm 10\%$ relative errors, as shown in Figure 19. By using the Darcy correlation, 63% and 70% of the wells were not in good agreement with the predicted and measured oil and water rate, respectively, with more than $\pm 18\%$ for relative errors, as shown in Figures 20 and 21. For predicted and measured gas rates, 79% of the wells showed more than $\pm 10\%$ relative errors, as shown in Figure 22. By using the Colebrook correlation, 67% and 75% of the wells were not in good agreement with the predicted and measured oil and water rate, respectively, with more than $\pm 18\%$ relative errors, as shown in Figures 23 and 24. For predicted and measured gas rates, 77% of the wells showed more than $\pm 10\%$ relative errors, as shown in Figure 25.

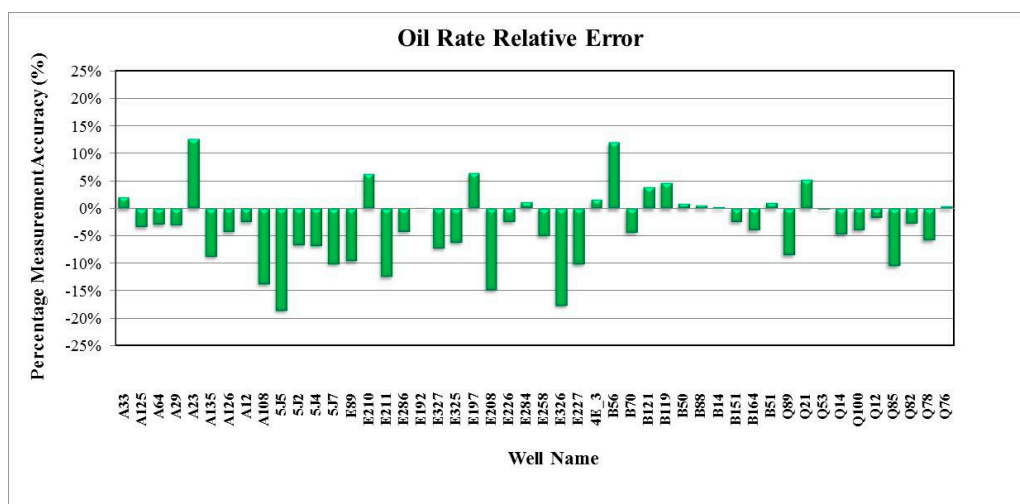


Figure 17. Oil rate measurement accuracy using the Blasius correlation.

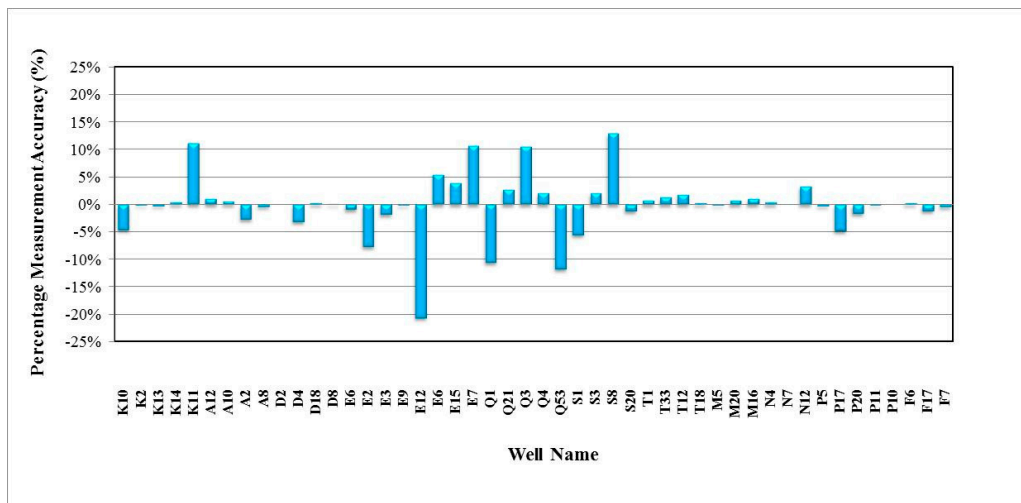


Figure 18. Water rate measurement accuracy using the Blasius correlation.

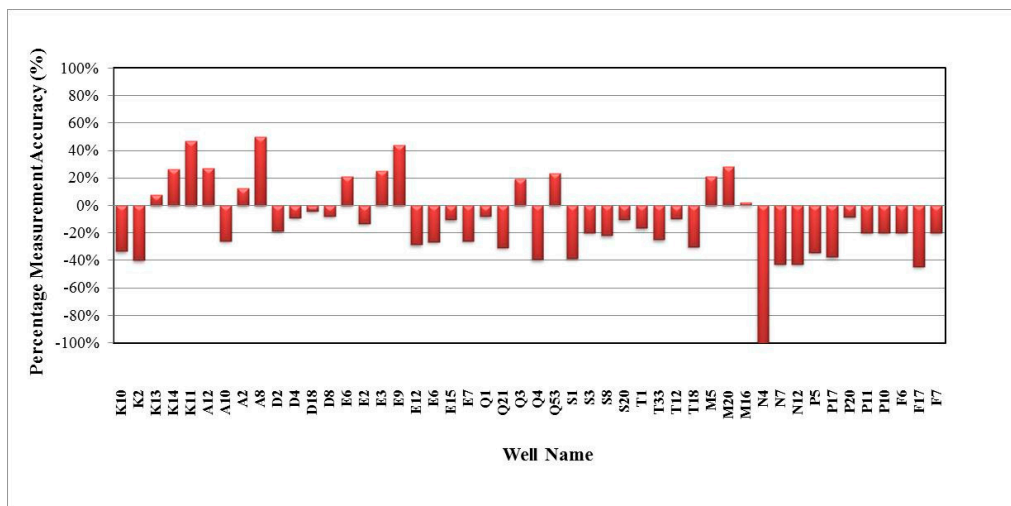


Figure 19. Gas rate measurement accuracy using the Blasius correlation.

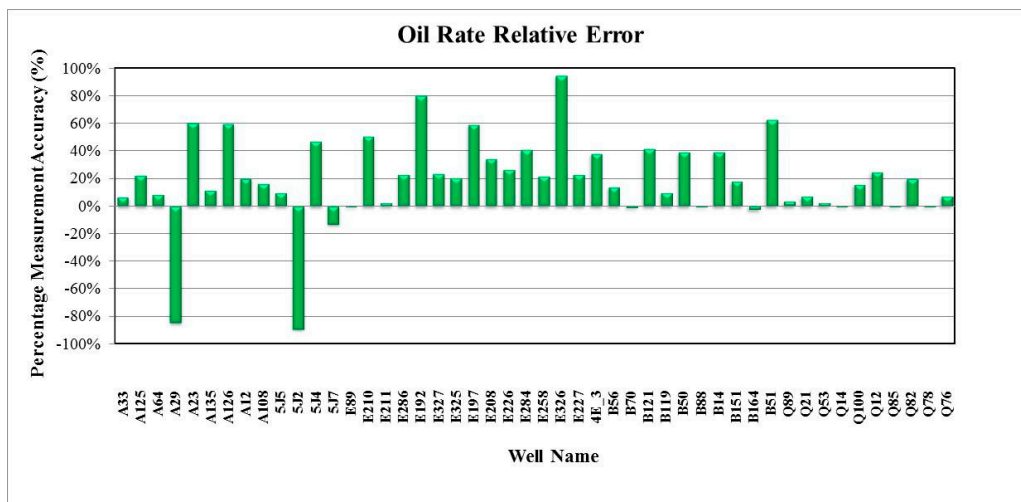


Figure 20. Oil rate measurement accuracy using the Darcy correlation.

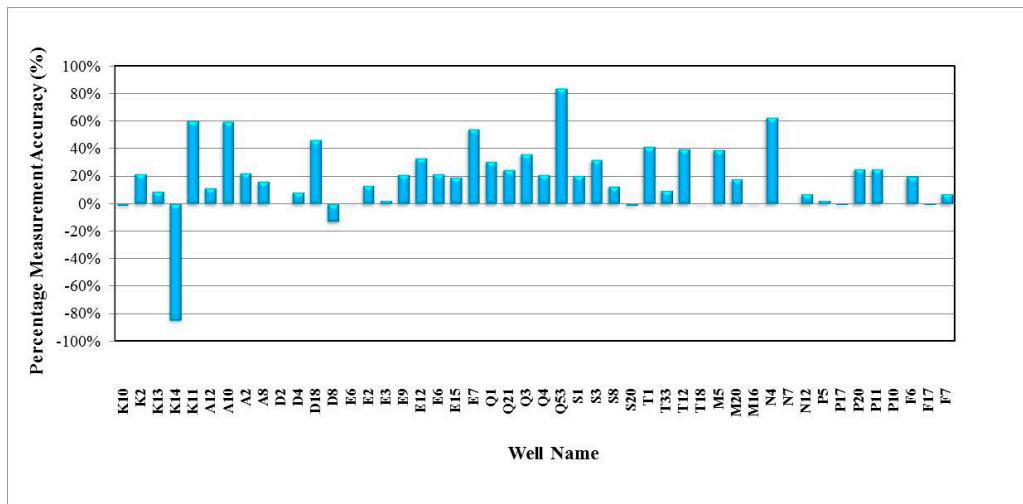


Figure 21. Water rate measurement accuracy using the Darcy correlation.

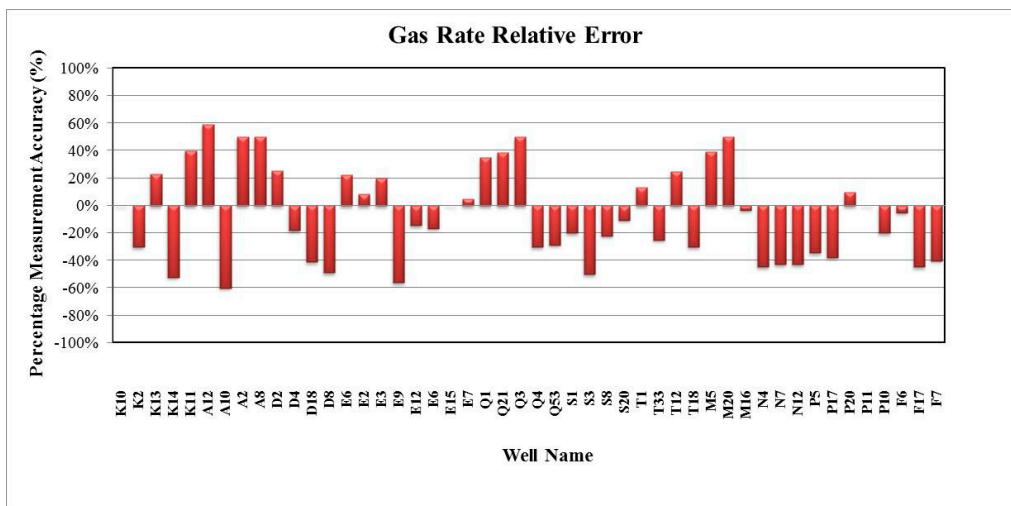


Figure 22. Gas rate measurement accuracy using the Darcy correlation.

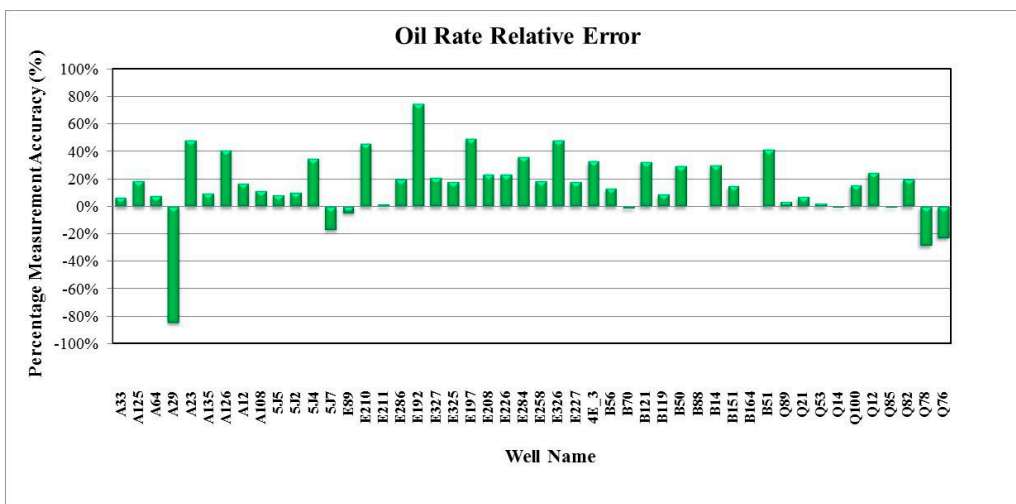


Figure 23. Oil rate measurement accuracy using the Colebrook correlation.

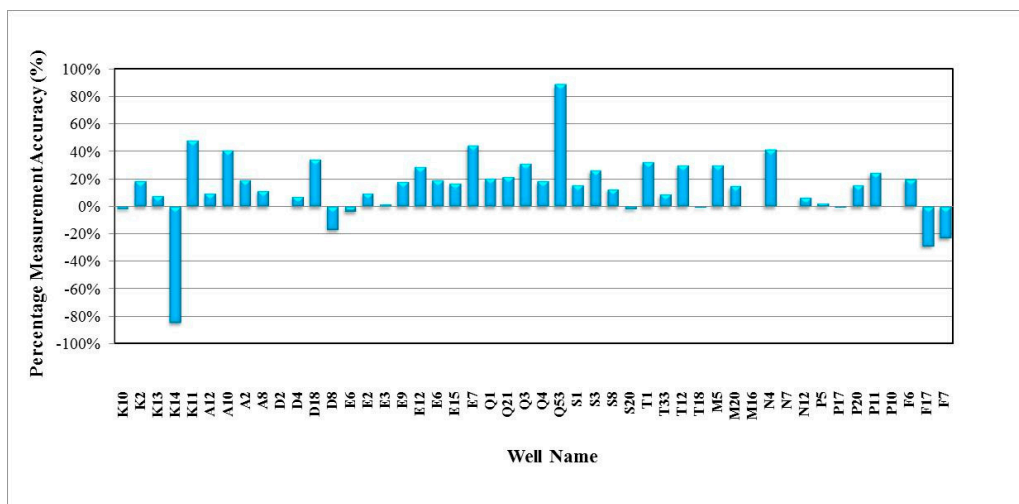


Figure 24. Water rate measurement accuracy using the Colebrook correlation.

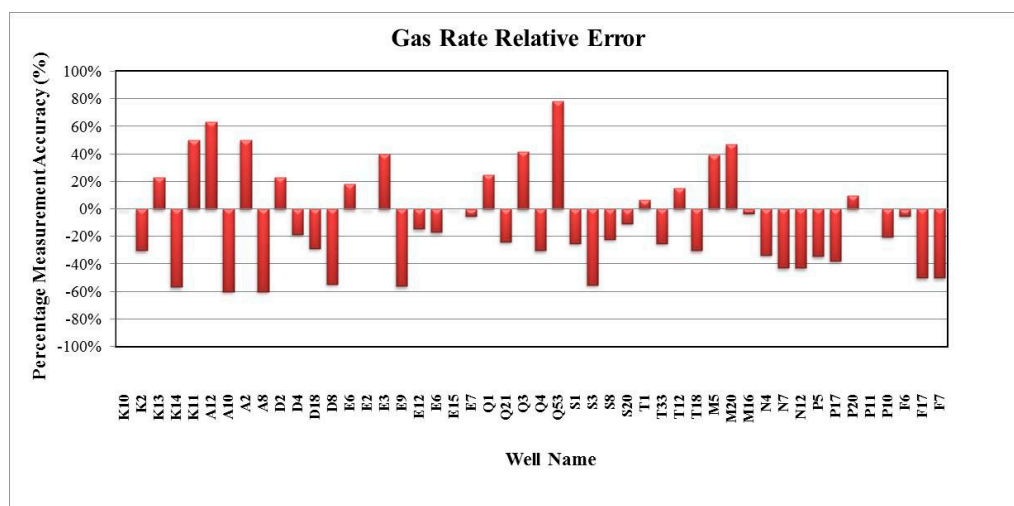


Figure 25. Gas rate measurement accuracy using the Colebrook correlation.

The results showed high relative errors in gas rate prediction which can happen due to the oil separator meters being insufficiently accurate. Also, these errors may occur due to fixed orifice plate meters used to measure the gas flow rate despite the fact that orifice plates are not appropriate to measure low gas rates. Besides, wear and corrosion can increase the orifice size and cause excessive loss.

4. Summary and Conclusions

The prediction of the fluid flow rate of oil wells using the new mathematical model has been made and validated with experimentally measured fluid flow rate data. To evaluate the influence of the frictional pressure drop value on the measurement of fluid flow rate of oil wells, Blasius, Darcy, and Colebrook friction correlations were applied. Using the Blasius correlation, the analysis showed that the predicted fluid flow rate values were in accord with the measured values, while by using the Darcy and Colebrook friction correlations, the results were not in good agreement with the measured values. This discrepancy was due to the fact that each friction correlation found the friction factor differently. To determine the friction factor, many expressions were used to compute the Reynolds number. Essentially, each empirical correlation states its own assumptions and modifications to defend the variable components in order to be applicable to multiphase conditions. The two-phase flow significantly complicated the pressure drop calculations, where any errors in determining the frictional

pressure drop values would generate some inaccuracies in predicting the fluid flow rate of the oil wells. Consequently, mixture properties and the interactions between the existing phase's properties must be considered. Therefore, the gas and liquid volume fractions throughout the conduit needed to be determined. Overall, the performance of the new mathematical model indicated that the selection of the appropriate friction factor correlation would lead to predicting the gas and liquid flow rate within the acceptable accuracy. However, the friction loss dominated only with very high flow rates. For relatively small flow rates, the hydrostatic pressure played the key role in the overall pressure drop in the vertical tubing. Thus, different multiphase flow models, either empirical or mechanistic model, used in the computation would output different predictions. That being said, the Blasius equation may be superior to other models coupled with the Hagedorn-Brown empirical correlation, as it has been shown in this work. Indeed, a very reasonable average relative error of 4.6% was observed between the predicted and measured flow rates. However, it may not be as good as it is when coupled with other mechanistic models that may further reduce this error. Further research is needed to further validate the developed model by accounting for other sophisticated multiphase models.

Author Contributions: T.A.G. derived the mathematical model, carried out the experimental validation and drafted the manuscript. M.H. contributed to data presentation, analysis of results and revision preparation.

Funding: The authors would like to acknowledge the Petroleum Engineering Department and Centre of Research in Enhanced Oil Recovery (COEOR) at Universiti Teknologi PETRONAS for the funding (YUTP-0153AA-E70) and the technical assistance.

Acknowledgments: Special thanks are due to production engineering staff of Waha Oil Company for their support. The authors also gratefully acknowledge assistance received from Lynn Mason for editing this manuscript.

Conflicts of Interest: The authors declare no conflict of interest.

Nomenclature

A	cross-sectional area, (sq ft)
API	American Petroleum Institute
B_o	oil formation volume factor, (bbl/stb)
B_{ob}	oil formation volume (at bubble point pressure), (bbl/STB)
B_g	gas formation volume factor, (cf/scf)
Cnt	count
dp/dz	pressure gradient, (psi/ft)
d	inside diameter, (ft)
ESP	electrical submersible pump
f	friction factor, (unitless)
g	Gravity, (ft/s ²)
H_L	liquid hold-up
H_G	gas hold-up
$H1$	bubble point pressure (at location depth before shut-in the well head valve), (ft)
$H2$	bubble point pressure (at location depth after shut-in the well head valve), (ft)
mt	mass flow rate, (lb/day)
N_{gv}	gas velocity number, (unitless)
N_{Lv}	liquid velocity number, (unitless)
N_d	pipe diameter number, (unitless)
N_{CL}	coefficient number of viscosity correction, (unitless)
N_L	liquid viscosity number, (unitless)
q_o	oil rate, (stb/day)
q_g	gas rate, (stb/day)
q_w	water rate, (stb/day)
q_L	liquid rate, (stb/day)

q_m	measured flow rate, (stb/day)
Q_C	quality check
P	pressure, (psia)
P_r	pseudo-critical pressure (for gas mixture), (psia)
P_b	bubble point pressure, (psia)
P_{sc}	pressure at standard conditions ($P = 14.7$ atm, $T = 60$ °F), (psia)
PSD	pump setting depth
SGG	gas specific gravity
STB	stock tank barrel (for liquid)
r_w	wellbore radius, (ft)
R_s	gas-oil ratio, (scf/stb)
R_{sb}	gas oil ratio at bubble point pressure, (cf/scf)
R_e	Reynolds number, (unitless)
T	temperature, (°F)
t	total shut-in time, (min)
T_r	pseudo-critical temperature (for gas mixture), (psia)
T_{sc}	temperature at standard condition, (°R)
T_r	reservoir fluid temperature, (°F)
VR	gas volume at reservoir conditions, (ft ³)
V_{sc}	gas volume at standard condition, (ft ³)
V_{SL}	superficial velocity for liquid, (ft/sec)
V_{Sg}	superficial velocity for gas, (ft/sec)
V_m	total mixture velocity, (ft/sec)
WHP_a	well head pressure (after shut-in the well), (psia)
WHP_b	well head pressure (before shut-in the well), (psia)
WC	water cut (unitless)
WHT	well head temperature, (°F)
W	water vapor density, (unitless)
Z	gas compressibility factor (unitless)
<i>Greek Symbols</i>	
ΔP	pressure drop, (psia)
H_L/ψ	hold-up correlation factor
γ_o	oil gravity
γ_w	water gravity
γ_g	gas gravity
σ	surface tension, (dyne/m)
ΔH	differences between bubble point pressure location depths (before and after shut-in the well head valve), (ft)
ρ_o	oil density, (lbm/ft ³)
ρ_g	gas density, (lbm/ft ³)
ρ_w	water density, (lbm/ft ³)
ρ_L	liquid density, (lb/ft ³)
ρ_m	mixture density, (lbm/ft ³)
μ_o	oil viscosity, cP
μ_g	gas viscosity, cP
μ_L	liquid viscosity, cP
<i>Subscripts</i>	
g_{sc}	gas (at standard condition)
h	hydrostatic
L	liquid
m	mixture (liquid and gas)
o	oil
sc	standard condition
w	water

References

1. Saeb, M.B.; Philip, D.M.; David, C.C.; Ali, J. Modeling friction factor in pipeline flow using a GMDH-type neural network. *Cogent Eng.* **2015**, *2*. [CrossRef]
2. Shannak, B.A. Frictional pressure drop of gas liquid two-phase flow in pipes. *Nuclear Eng. Des.* **2008**, *238*, 3277–3284. [CrossRef]
3. Jiang, J.Z.; Zhang, W.M.; Wang, Z.M. Research progress in pressure-drop theories of gas-liquid two-phase pipe flow. In Proceedings of the China International Oil & Gas Pi (CIPC 2011), Langfang, China, 5 September 2011.
4. Xu, Y.; Fang, X.D.; Su, X.H.; Zhou, Z.R.; Chen, W.W. Evaluation of frictional pressure drop correlations for two-phase flow in pipes. *Nuclear Eng. Des.* **2012**, *253*, 86–97. [CrossRef]
5. Mittal, G.S.; Zhang, J. Friction factor prediction for Newtonian and non-Newtonian fluids in pipe flows using neural networks. *Int. J. Food Eng.* **2007**, *3*, 1–18. [CrossRef]
6. Fadare, D.A.; Ofidhe, U.I. Artificial neural network model for prediction of friction factor in pipe flow. *J. Appl. Sci.* **2009**, *5*, 662–670.
7. Bilgil, A.; Altun, H. Investigation of flow resistance in smooth open channels using artificial neural networks. *Flow Meas. Instrum.* **2008**, *19*, 404–408. [CrossRef]
8. Özger, M.; Yildirim, G. Determining turbulent flow friction coefficient using adaptive neuro-fuzzy computing techniques. *Adv. Eng. Softw.* **2009**, *40*, 281–287. [CrossRef]
9. Shayya, W.H.; Sablani, S.S.; Campo, A. Explicit calculation of the friction factor for non-Newtonian fluids using artificial neural networks. *Dev. Chem. Eng. Miner. Process.* **2005**, *13*, 5–20. [CrossRef]
10. Yuhong, Z.; Wenxin, H. Application of artificial neural network to predict the friction factor of open channel flow. *Commun. Nonlinear Sci. Numer. Simul.* **2009**, *14*, 2373–2378. [CrossRef]
11. Yazdi, M.; Bardi, A. Estimation of friction factor in pipe flow using artificial neural networks. *Can. J. Autom. Control Intell. Syst.* **2011**, *2*, 52–56.
12. Sablani, S.S.; Shayya, W.H. Neural network based non-iterative calculation of the friction factor for power law fluids. *J. Food Eng.* **2003**, *57*, 327–335. [CrossRef]
13. Griffith, P. Two-Phase Flow in Pipes. In *Special Summer Program*; Massachusetts Institute of Technology: Cambridge, MA, USA, 1962.
14. Raxendell, P.B. The Calculation of Pressure Gradients in High-Rate Flowing Wells. *J. Pet. Technol.* **1961**, *13*, 1023. [CrossRef]
15. Fancher, G.H.; Brown, K.E. Prediction of Pressure Gradients for Multiphase Flow in Tubing. *Soc. Pet. Eng. J.* **1963**, *3*, 59. [CrossRef]
16. Hagedorn, A.R.; Brown, K.E. The Effect of Liquid Viscosity in Vertical Two-Phase Flow. *J. Pet. Technol.* **1964**, *16*, 203. [CrossRef]
17. Poettmann, F.H.; Carpenter, P.G. The Multiphase Flow of Gas, Oil and Water through Vertical Flow Strings with Application to the Design of Gas-Lift Installations. In Proceedings of the Drilling and Production Practice, New York, NY, USA, 1 January 1952; Volume 52, p. 257.
18. Tek, M.R. Multiphase Flow of Water, Oil and Natural Gas Through Vertical Flow Strings. *J. Pet. Technol.* **1961**, *13*, 1029. [CrossRef]
19. Shaban, H.; Tavoularis, S. Identification of flow regime in vertical upward air–water pipe flow using differential pressure signals and elastic maps. *Int. J. Multiph. Flow* **2014**, *61*, 62–72. [CrossRef]
20. Daev, Z.A.; Kairakbaev, A.K. Measurement of the Flow Rate of Liquids and Gases by Means of Variable Pressure Drop Flow Meters with Flow Straighteners. *Meas. Tech.* **2017**, *59*, 1170–1174. [CrossRef]
21. Cai, B.; Guo, D.X.; Jing, F.W. Study on gas-liquid two-phase flow patterns and pressure drop in a helical channel with complex section. In Proceedings of the 23rd International Compressor Engineering Conference, West Lafayette, IN, USA, 11–14 July 2016.
22. Oliveira, J.L.G.; Passos, J.C.; Verschaeren, R.; Van der Geld, C. Mass flow rate measurements in gas-liquid flows by means of a venturi or orifice plate coupled to a void fraction sensor. *Exp. Therm. Fluid Sci.* **2009**, *33*, 253–260. [CrossRef]
23. Brown, G.O. The history of the Darcy-Weisbach equation for pipe flow resistance. *Environment*. Available online: <https://ascilibrary.org/doi/abs/10.1061/40650> (accessed on 17 September 2018).
24. Blasius, H. *Das Ähnlichkeitsgesetz bei Reibungsvorgängen in Flüssigkeiten, Mitteilung 131 über Forschungsarbeiten auf dem Gebiete des Ingenieurwesens*; Springer: Berlin, Germany, 1913.

25. Colebrook, C.F. Turbulent flow in pipes, with particular reference to the transition region between the smooth and rough pipe laws. *J. Inst. Civ. Eng.* **1939**, *11*, 133–156. [[CrossRef](#)]
26. Lee, A.L.; Gonzalez, M.H.; Eakin, B.E. The Viscosity of Natural Gases. *J. Pet. Technol.* **1966**, *18*, 997–1000. [[CrossRef](#)]
27. Beggs, D.H.; Brill, J.P. A study of two-phase flow in inclined pipes. *J. Pet. Technol.* **1973**, *25*, 607–617. [[CrossRef](#)]
28. Standing, M.B.; Katz, D.L. Density of natural gases. *Trans. AIME* **1942**, *146*, 140–149. [[CrossRef](#)]
29. Sloan, E.; Houry, F.; Kobayashi, R. Measurement and interpretation of the water content of a methane-propane mixture in the gaseous state in equilibrium with hydrate. *Ind. Eng. Chem. Fundam.* **1982**, *21*, 391–395.
30. Vazquez, M.; Beggs, H.D. Correlations for Fluid Physical Property Prediction. *J. Pet. Technol.* **1980**, *32*, 968–970. [[CrossRef](#)]
31. Hagedorn, A.R.; Brown, K.E. Experimental Study of Pressure Gradients Occurring during Continuous Two-Phase Flow in Small Diameter Vertical Conduit. *J. Pet. Technol.* **1965**, *17*, 475–484. [[CrossRef](#)]
32. Duns, H., Jr.; Ros, N. Vertical Flow of Gas and Liquid Mixtures in Wells. In Proceedings of the 6th World Petroleum Congress, Frankfurt am Main, Germany, 19–26 June 1963; p. 451.
33. Orkiszewski, J. Predicting Two-Phase Pressure Drops in Vertical Pipe. *J. Pet. Technol.* **1967**, *19*, 829–838. [[CrossRef](#)]
34. Aziz, K.; Govier, G.; Fogarasi, M. Pressure Drop in Wells Producing Oil and Gas. *J. Can. Pet. Technol.* **1972**, *11*, 38. [[CrossRef](#)]



© 2018 by the authors. Licensee MDPI, Basel, Switzerland. This article is an open access article distributed under the terms and conditions of the Creative Commons Attribution (CC BY) license (<http://creativecommons.org/licenses/by/4.0/>).